A&A 382, 17–27 (2002)
DOI: 10.1051/0004-6361:20011665

Astronomy & Astrophysics

SC 1327–312 & SC 1329–313: Two galaxy groups in-between a major merging event observed with Beppo–SAX

S. Bardelli[1], S. De Grandi[2], S. Ettori[3], S. Molendi[4], E. Zucca[1], and S. Colafrancesco[5]

[1] Osservatorio Astronomico di Bologna, via Ranzani 1, 40127 Bologna, Italy
[2] Osservatorio Astronomico di Brera, Via Bianchi 46, 23807 Merate (LC), Italy
[3] Institute of Astronomy, Madingley Road, CB3 0HA Cambridge, UK
[4] Istituto di Fisica Cosmica "G. Occhialini", Via Bassini 15, 20133 Milano, Italy
[5] Osservatorio Astronomico di Roma, via Frascati 33, 00040 Monteporzio Catone, Italy

Received 1 August 2001 / Accepted 18 October 2001

Abstract. We present the results of two Beppo-SAX observations of the poor clusters SC 1327–312 and SC 1329–313: these objects are located in a huge structure, formed by three ACO clusters, which is probably the remnant of one of the largest and best studied major mergings known. Given the fact that these poor clusters are in between two interacting ACO clusters, the aim of this work is to study the physics of the intracluster medium and to look for the possible presence of shocks. We derived the gas distribution profiles, the global (i.e. within 0.3 h^{-1} Mpc) temperatures and abundances and the temperature profiles and maps for SC 1327–312 and SC 1329–313. Also the presence of soft excess in LECS and hard excess in PDS have been examined. We do not find evidence of regions where the gas is shocked or significantly heated. The image of SC 1327–312 seems rather symmetric, while the gas profile of SC 1329–313 shows disturbed, "comet-like" shaped isophotes, with the tail pointing toward A3562 and a compression toward SC 1327–312. The presence of multiphase gas in SC 1329–313, as claimed by Hanami et al. (1999) based on ASCA data, has been found only at the 2σ confidence level. The lack of heating supports the hypothesis that the merging is at a late stage, after the first core–core encounter, when the main shock front had the time to travel to the external regions of the main clusters.

Key words. X-rays: galaxies: clusters – galaxies: clusters: general galaxies: clusters: individual: SC1327–312 – galaxies: clusters: individual: SC1329–313

1. Introduction

Cluster mergings are among the most energetic phenomena in the Universe, leading to a release of $\sim 10^{50-60}$ erg on a time scale of the order of few Gyrs (Sarazin 2000), but it is not yet clear in detail in which way this kinetic energy is dissipated and what its influence on the galaxy population is. There are some observational features that have been associated with the cluster merging phenomenon, like shocks in the hot gas, radio halos, relics and wide angle tail radiosources, and the presence of starburst activity in galaxies, although the precise theoretical description is not yet completely assessed.

The main difficulty in understanding the merging phenomenon is that the available data allow only studies focussed on single events, mainly in cases where the intervening entity has a much smaller mass with respect to the main cluster. Moreover, some authors limited the analysis to single wavelengths (in particular X-ray band): however, although the X-ray band is very powerful for these studies, a multiwavelength analysis would give a more global view of the phenomenon.

Another important point is the key role played by the large–scale environment. It has been recognized from cosmological simulations that rich clusters are accreting groups and other clusters along filaments (Colberg et al. 1999), which determine the relative velocity and frequency of the impacts. Rich superclusters are places where one can find the most spectacular cases of such dynamical phenomena: the peculiar velocities due to the enhanced local density favour cluster-cluster collisions, i.e. involving entities of similar mass (hereafter "major mergings").

The most remarkable examples of cluster mergings are found in the central region of the Shapley Concentration, the richest supercluster of clusters within 300 h^{-1} Mpc (Zucca et al. 1993). At the center of the Shapley Concentration we individuated (Bardelli et al. 1994) two cluster structures (on scales of ~ 5 h^{-1} Mpc) which are cluster-cluster mergings at two different stages. The most massive structure (dubbed A3558 complex,

Send offprint requests to: S. Bardelli,
e-mail: bardelli@bo.astro.it

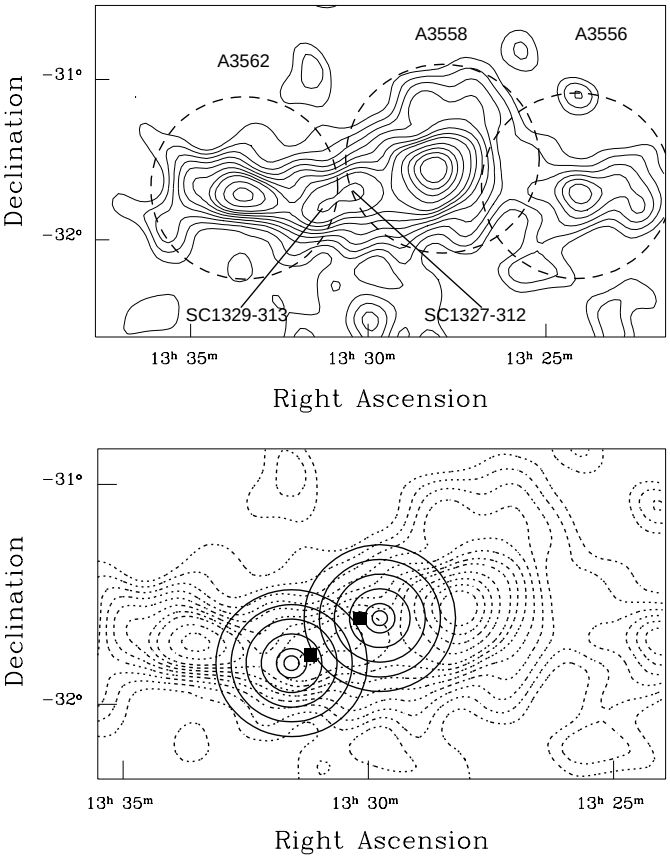

Fig. 1. Upper panel: optical galaxy isodensity contours of the A3558 cluster complex. The data have been smoothed with a Gaussian of 6 arcmin of *FWHM*. Circles of 1 Abell radius have been drawn as dashed curves around each cluster and the optical position of SC 1327–312 and SC 1329–313 is indicated. Lower panel: close up of the same region, with superimposed the Beppo-SAX fields. Concentric annuli correspond to the regions analyzed in Sects. 4.2 and 5.2. Solid squares indicate the position of the optical three-dimensional substructures associated to SC 1327–312 (T478 on the right) and to SC 1329–313 (T520 on the left), found by Bardelli et al. (1998b); see the text for more details.

Bardelli et al. 1994, 1998a) is probably a merging seen just after the first core-core encounter. The other complex, dominated by A3528, is formed by two pairs of clusters and is probably at the first stages of interaction (Bardelli et al. 2001; Baldi et al. 2001).

In this paper we present the analysis of Beppo-SAX observations pointed on the poor clusters SC 1327–312 and SC 1329–313, placed in the A3558 complex at the expected position of the shock front.

The plan of the paper is the following. In Sect. 2 we describe the characteristics of the A3558 complex and in Sect. 3 we give details about observations and data reduction. In Sects. 4 and 5 we present the analysis of SC 1327–312 and SC 1329–313, respectively; in Sect. 6 we look for the possible existence of a soft excess in the Beppo-SAX LECS data, while the analysis of Beppo-SAX PDS data is given in Sect. 7. Finally, in Sect. 8 we discuss and summarize the results.

2. The A3558 cluster complex

The A3558 complex (Bardelli et al. 1994) is a chain of clusters almost perpendicular to the line of sight, spanning $\sim 7\ h^{-1}$ Mpc at a redshift of ~ 0.05, and is formed by three ACO clusters (A3558, A3562 and A3556) and two poor groups (dubbed SC 1327–312 and SC 1329–313 by Breen et al. 1994). This structure represents a density excess in number of galaxies of $N/\bar{N} \sim 45$, comprising a total mass in the range $\sim 1-5 \times 10^{15}\ h^{-1}\ M_{\odot}$ (Bardelli et al. 2000). A simple dynamical model shows that, with these characteristics, the complex is expected to be in the late stage of collapse.

From the two-dimensional distribution of optical galaxies (Fig. 1) and a redshift survey of ~ 700 galaxies, we found that the external objects seem to form an envelope sourronding the cluster cores (Bardelli et al. 1994, 1998a). Detailed substructure analysis (Bardelli et al. 1998b) revealed a large number of subclumps, suggesting that the complex is far from a relaxed state.

Considering the X-ray band, Bardelli et al. (1996) and Kull & Böhringer (1999) showed that the whole chain is embedded in a hot gas filament. The clusters of the chain have been extensively studied as single entities (Bardelli et al. 1996; Ettori et al. 1997; Markevitch et al. 1998; Hanami et al. 1999; Ettori et al. 2000), finding evidences of disturbance.

Remarkable results are found also in the radio band (Venturi et al. 2000): comparing the bivariate radio-optical luminosity function of radiogalaxies in this complex with that of radiogalaxies in a sample of "normal" clusters (Ledlow & Owen 1996), we found a significant lack of radiosources. It seems that the cluster interaction "switched off" the central engines of the AGNs. Moreover, a relic of radiogalaxy has been found at the edge of a probably merging event between A3556 and a smaller group, projected along the line of sight (Venturi et al. 1998).

In order to explain these facts, we adopted the working hypothesis that the A3558 complex is the remanant of a cluster-cluster collision seen just after the first core-core encounter (Bardelli et al. 1998b). We speculated that a cluster collided with A3558 and its remnants are visible as the overdensity regions of SC 1327–312, SC 1329–313 and A3562. In this framework, A3556 would be formed by the members of the intervening cluster remained in the backside part of the merging direction. Therefore, all galaxies outside A3558 would belong to the destroyed cluster and form the clumpiness expected from the simulations.

Hydrodynamical simulations have shown that mergers usually produce shocks in the intracluster medium (see e.g. Sarazin 2000; Roettiger et al. 1997; Takizawa & Mineshige 1998; Ricker & Sarazin 2001): at early stages, the shocked region is located between the nuclei of the impacting clusters, while at later times the shocks sweep over the centers and reach the outer regions.

In order to completely understand the chain of events that created the A3558 complex and in particular the time scale of the merging, it is important to try to locate the

locus of the shock (if present). The most natural place to be explored is the region between A3562 and A3558, where the two poor clusters SC 1327–312 and SC 1329–313 are located.

3. Observations and data reduction

The clusters SC 1327–312 and SC 1329–313 were observed by the Beppo-SAX satellite (Boella et al. 1997a) in the periods 1999 December 28–30 and 2000 January 15–18, respectively. We discuss here the data from two of the instruments onboard Beppo-SAX: the Medium-Energy Concentrator Spectrometer (MECS) and the Low-Energy Concentrator Spectrometer (LECS). The MECS (Boella et al. 1997b) is presently composed of two units, working in the [1–10] keV energy range. At 6 keV, the energy resolution is ∼8% and the angular resolution is ∼0.7′ (*FWHM*). The LECS (Parmar et al. 1997), consists of an imaging X-ray detector, working in the [0.1–9] keV energy range, with 20% spectral resolution and 0.8′ (*FWHM*) angular resolution (both computed at 1 keV). Standard reduction procedures and screening criteria have been adopted to produce linearized (i.e. corrected for intrinsic distorsion of the detector), cleaned (filtered to remove non-scientific event and to correct gain variations) and equalized (in order to report the two MECS at the same energy scale) event files. The MECS (LECS) data preparation and linearization was performed using the SAXDAS (SAXLEDAS) package under FTOOLS environment.

We have taken into account the PSF-induced spectral distortions (D'Acri et al. 1998) in the MECS analysis using effective area files produced with the *effarea* program. All MECS spectra have been background subtracted using spectra extracted from blank sky event files in the same region of the detector as the source (see Fiore et al. 1999). A detailed explanation of the MECS analysis is given in De Grandi & Molendi (2001): in the following we'll concentrate on the most important steps. As done in Ettori et al. (2000), for the LECS we have used two redistribution matrices and ancillary response files, the first computed for an on-axis pointlike source and the second for a source with a flat brightness profile. The temperatures and abundances we derive in the two cases do not differ significantly, as the telescope vignetting in the [0.1–4.0] keV energy range is not strongly dependent upon energy. All spectral fits have been performed using XSPEC Ver. 10.00.

The observation log is reported in Table 1 and the field position is shown in the lower panel of Fig. 1. The observed count–rates for SC 1327–312 and for SC 1329–313 for the 2 MECS units and within the central 8 arcmin (corresponding to 0.33 h^{-1} Mpc) are 0.122 cts s^{-1} and 0.060 cts s^{-1}, respectively. For the LECS data, the count–rates in the same region are 0.087 and 0.045, respectively.

4. SC 1327–312

The cluster SC 1327–312 ($\alpha_{2000} = 13^{\rm h}29^{\rm m}47^{\rm s}$, $\delta_{2000} = -31°36'29''$, from Bardelli et al. 1996) is located

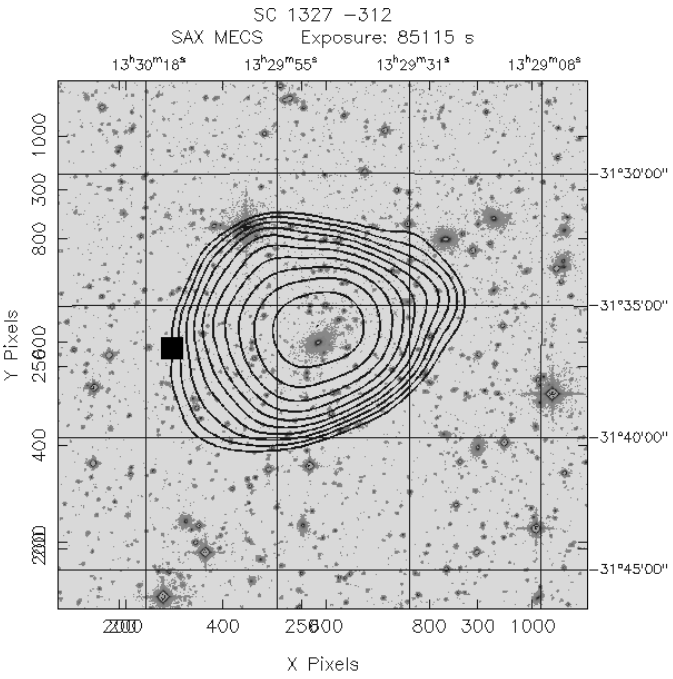

Fig. 2. MECS image of SC 1327–312 in the [2–10] keV energy range. The data have been smoothed with a Gaussian of 6 pixels, corresponding to 0.8 arcmin. In this figure we show the X-ray contours from the central region of 8 arcmin radius, superimposed to the Digital Sky Survey. The solid square indicates the position of the optical group T478 (see the caption of Fig. 1 and the text for more details).

23.6 arcmin (∼1 h^{-1} Mpc) from the center of the dominant cluster A3558. In Fig. 2 the isodensity contours of the MECS image (in the energy range [2–10] keV) are reported, after having applied a smoothing of 6 pixels, corresponding to 0.8 arcmin. The X-ray emission from the central 8 arcmin is overplotted on the optical data taken from the Digital Sky Survey: the emission seems to be symmetric and centered on the brightest galaxy, which has $b_{\rm J} = 15.6$ and $v = 15\,121$ km s^{-1}. The distribution of optical galaxies does not show a clear overdensity at the position of this group: the nearest group found by the three-dimensional substructure analysis of Bardelli et al. (1998b), dubbed T478, is ∼5 arcmin away from the X-ray position, in the East direction (see lower panel of Figs. 1 and 2). This offset could be due to the contamination of galaxies from the nearby cluster A3558, which decreases the significance of the optical overdensity. Moreover the optical isodensity distribution in this region shows a dependence on the magnitude range (see Fig. 14 of Bardelli et al. 1994), another indication of possible contamination from nearby structures.

This group appears in a ROSAT-PSPC observation pointed on A3558: unfortunately, is has been observed off-axis, where the spatial resolution is strongly degraded; moreover its emission is disturbed by the presence of a supporting rib of the detector (see Bardelli et al. 1996). For this reason, we fitted an elliptical King model (i.e.

Table 1. Beppo-SAX observation log (data are referred to MECS).

Target	α (2000) h m s	δ (2000) ° ′ ″	date	exp.time ksec	count–rate cts/s
SC 1327–312	13 29 47	−31 36 29	1999 Dec. 28–30	85.1	0.122
SC 1329–313	13 31 36	−31 48 46	2000 Jan. 15–18	130.2	0.060

with two core radii, see Bardelli et al. 1996) directly to the Beppo-SAX MECS image.

We found that the best fit within a region of 8 arcmin radius is $r_{c1} = 0.101\ h^{-1}$ Mpc, $r_{c2} = 0.135\ h^{-1}$ Mpc and $\beta = 0.492$. Note that the core radius values correspond to ∼4 times the resolution and could be considered an unbiassed measure.

In order to explore the dependence of the results on the PSF, we deconvolved the image with a Clark Clean Method, finding that the parameters vary by a 5%, in the sense of reducing the core radii.

The only value present in the literature is $r_c = 0.17 \pm 0.01\ h^{-1}$ Mpc obtained by Breen et al. (1994) on Einstein-IPC data, fixing the slope to $\beta = 0.6$. With our parameters and using the estimated global temperature of the hot gas (see below), the total mass is $M(<1\ h^{-1}\ \mathrm{Mpc}) \sim 2.0 \times 10^{14}\ h^{-1}\ M_\odot$, with a baryonic fraction of ∼7% $h^{-1.5}$.

The luminosity resulted to be $3.76 \times 10^{43}\ h^{-2}$ erg s^{-1} in the [2–10] keV band and $1.77 \times 10^{43}\ h^{-2}$ erg s^{-1} in the [0.6–3] keV band. These values have been estimated within a distance of $0.5\ h^{-1}$ Mpc from the cluster center.

4.1. Global temperature and abundance

In order to find the global temperature, we extracted a circular region of 8 arcmin from the center of the MECS data in the range [2–10] keV. We fitted the spectrum with a *mekal* (Mewe et al. 1995; Kaastra 1992) model with an absorbing Galactic hydrogen column (*wabs* model), as implemented in the XSPEC package. After having checked that the fitted Galactic absorption is consistent with the literature measurement of 3.88×10^{20} cm^{-2} (Dickey & Lockman 1990), we fixed it to this latter value. The results are reported in Table 2.

In order to use all the information present in the Beppo-SAX observation, we added the data of the LECS instrument in the [0.6–3] keV band. From a ROSAT-PSPC image, Bardelli et al. (1996) found that superimposed on the cluster image (at ∼4.6 arcmin from the cluster center) there is a K1 III star (SAO 204527 or HD 117310), whose X-ray emission is well fitted by a Raymond-Smith model with $kT = 1.10$ keV. This emission is likely affecting only the LECS energy range: for this reason we fitted the *mekal* model adding a Raymond-Smith model with $kT = 1.10$ keV and abundance of 0.20. The resulting temperature is $4.11^{+0.43}_{-0.36}$ keV and the abundance is $0.17^{+0.08}_{-0.08}$, with a reduced χ^2 of 1.03 with 189 degrees of freedom. However, neglecting the star contribution, the results are very similar, with a reduced χ^2 of 1.05 with 192 degrees of freedom. Also these results are reported in Table 2.

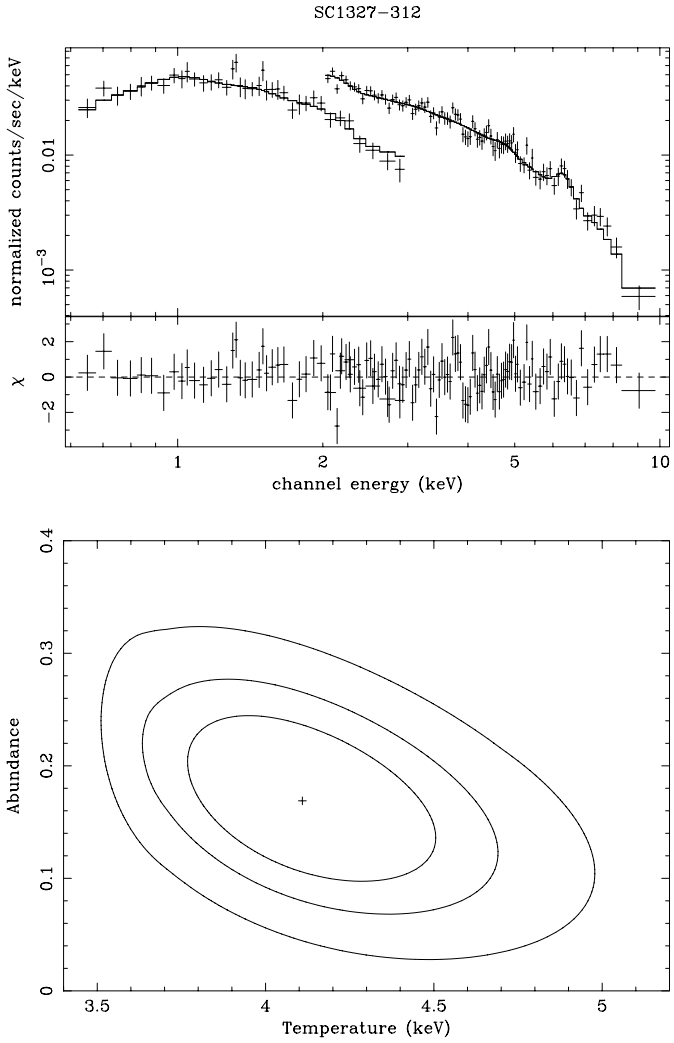

Fig. 3. Spectrum and confidence ellipse of the estimated temperature and abundance on MECS+LECS data within 8 arcmin from the center of SC 1327–312.

In Fig. 3 we show the combined LECS+MECS spectrum of SC 1327–312, overplotted to the fit, and the corresponding confidence ellipse of the temperature and abundance parameters. The value of the temperature is in agreement with the determination of $kT = 3.85$ keV from ROSAT-PSPC (Bardelli et al. 1996) and is consistent at 1.5 sigma with the ASCA determinations of $kT = 3.76 \pm 0.13$ keV (Hanami et al. 1999).

Following the $\sigma - T$ relation of Lubin & Bahcall (1993) [$\sigma = 332(kT)^{0.6}$ km s^{-1}], the determined temperature

Table 2. Spectral results from a region of 8 arcmin from the center of SC 1327–312 and SC 1329–313. Errors are 90% confidence level.

Object	kT (keV)	Abundance	Reduced χ^2 (d.o.f.)
SC 1327–312 MECS	$3.93^{+0.16}_{-0.17}$	$0.17^{+0.05}_{-0.04}$	1.05 (133)
SC 1327–312 LECS+MECS	$4.11^{+0.43}_{-0.36}$	$0.17^{+0.08}_{-0.08}$	1.03 (189)
SC 1329–313 MECS	$3.43^{+0.28}_{-0.25}$	$0.22^{+0.11}_{-0.11}$	1.02 (125)
SC 1329–313 LECS+MECS	$3.49^{+0.27}_{-0.24}$	$0.21^{+0.09}_{-0.11}$	0.92 (181)

implies a velocity dispersion of 775^{+47}_{-41} km s^{-1}, consistent with the value of Bardelli et al. (1998a) of 691^{+158}_{-246} km s^{-1}.

4.2. MECS spatially resolved spectroscopy

The cluster emission in the central 8 arcmin circle has been divided into 2′ wide concentric annuli, centered on the X-ray emission peak. To all spectra accumulated from these annular regions, we have applied a single temperature model (i.e. *mekal* model) absorbed for the nominal Galactic hydrogen column density (*wabs* model) to derive temperature and metal abundances. The adopted column density for SC 1327–312 is 3.88×10^{20} cm^{-2} (see Sect. 4.1), and the energy range considered for the spectral fitting procedure is [2–10] keV.

In Fig. 4 we report the temperature and abundance profiles of SC 1327–312 in annuli around the cluster center. The vertical bars correspond to the 68% errors and the horizontal bars represent the bins used to extract the counts. For the last point, for which the abundance is not constrainted, we fixed it at the value of the global fit, i.e. 0.17. For this reason this last abundance point is plotted without error bars. If we extrapolate the abundance profile with a linear fit (see below), we obtain the value indicated with the square: in the temperature plot, the square indicates the kT derived using this abundance value. These points were plotted in order to give a feeling of the dependence of the fitted temperature on the abundance determination. Finally, dotted lines correspond to the values obtained from the global fit.

The temperature profile appears to be constant, a part a weak indication of a decrease in the most central bin: averaging the values of all bins we find $kT = 3.88^{+0.15}_{-0.16}$ keV, well in agreement with the global fitted temperature. On the contrary, the abundance seems to present a decreasing trend. In order to extrapolate the trend to the 6−8 arcmin bin, we fitted the linear relation $(0.33-0.041r)$.

We have performed two-dimensional spectral analysis of SC 1327–312 by extracting spectra from sectors of annuli as shown in Fig. 5: out to 4 arcmin each annulus is 2′ wide, beyond this radius the annuli are 4′ wide. This figure shows the MECS image of the cluster with the four sectors overlaid: note that the contours shown in Fig. 2 correspond only to the inner part of this plot. We have tilted the sectors with a position angle (measured from North to East) of 60 degrees in order to have the North-West sector pointing toward A3558 and the South-East

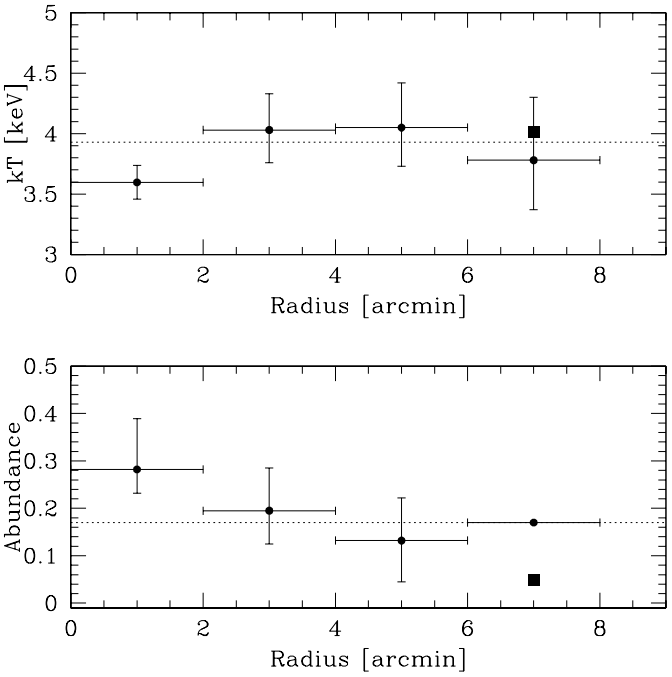

Fig. 4. Temperature and abundance radial profile of SC 1327–312. The vertical bars correspond to 68% errors, while the horizontal bars represent the bins used to extract the counts. Dotted lines indicate the global fit values. Squares are values obtained by fixing the abundance value at the linear extrapolation of the abundance profile.

one toward SC 1329–313. The considered energy band is again [2–10] keV, except for the 8′−12′ annulus. In this annulus we have applied a correction for the absorption caused by the strongback supporting of the detector window and in this case the energy range is [3.5–10] keV to avoid the low energy part of the spectrum, where the correction for the strongback is less reliable.

In Fig. 6 we show the temperature profiles derived for SC 1327–312 from the spectral fits for each of the 4 sectors. In all profiles we have included the temperature obtained for the central circular region with radius 2′. The radial temperature profile for each sector stops at the last annulus where the source counts are more than 30% of the total (i.e. source plus background) counts. This is the reason why there are different radial extensions for the profiles in the four quadrants: in the outermost bins in the North-West and South-East sectors there is a contribution from the emission of the adjacent clusters.

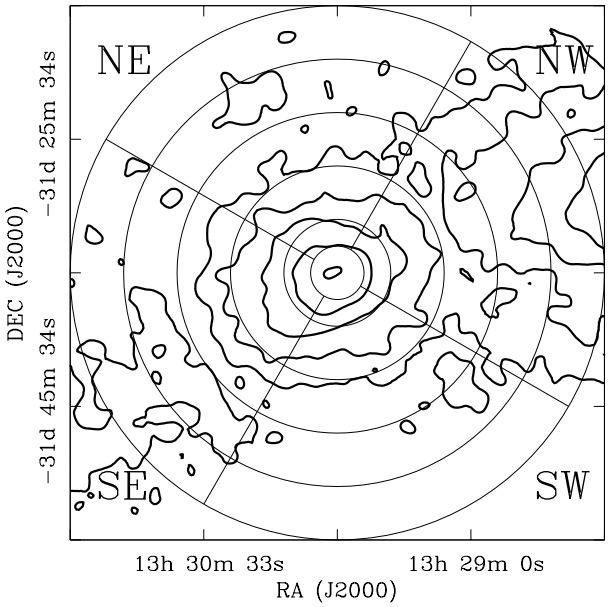

Fig. 5. Beppo-SAX MECS image of SC 1327–312. Contour levels (thick lines) are spaced logarithmically. Overlapped to the contours the concentric circles and the cross, drawn as thinner lines, show how the cluster has been divided to obtain temperature maps. The position angle (computed from North to East) is 60°. The NW sector is pointing toward A3558 and the SE one toward SC 1329–313. Note that the effect of the supporting structure of the MECS entrance window (i.e. the strongback) has been not corrected in this images.

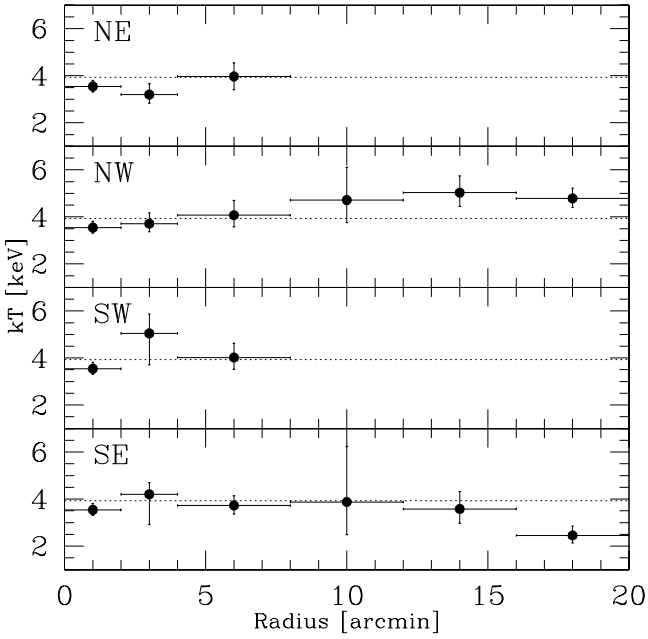

Fig. 6. Two-dimensional radial profile of the temperature of SC 1327–312. The four panels show the results of the four sectors indicated in Fig. 5. The vertical bars correspond to one sigma errors, while the horizontal bars represent the bins used to extract the counts. Dotted lines indicate the global fit values.

More specifically, sector North-West points toward A3558, a cluster at a global temperature of 5.5 keV (Markevitch & Vikhlinin 1997), which is about 24 arcmin away from SC 1327–312 (note that our measurements extend up to 20 arcmin from the cluster center only). Markevitch & Vikhlinin (1997) measured the temperature map for A3558 using ASCA data: they find a temperature of about 4.0 ± 0.8 keV (90% c.l. errors) in their sector of annulus pointing towards SC 1327–312 (i.e. region 9 in Fig. 2 of Markevitch & Vikhlinin 1997), in agreement with the mean temperature we find for the three outermost bins of sector North-West, i.e. 4.7±0.6 keV (90% c.l.). We have fitted the temperature in sector North-West with a constant kT model, finding a mean temperature of 4.0 ± 0.2 with a reduced $\chi^2 = 1.6$; we find a marginal (at ∼98% c.l. using the F-test) evidence of temperature increase from 0 to 20 arcmin by fitting the data with a linear model. At the scales considered here we can exclude strong temperature enhancements along this direction.

5. SC 1329–313

The cluster SC 1329–313 ($\alpha_{2000} = 13^{\rm h}31^{\rm m}36^{\rm s}$, $\delta_{2000} = -31°48'46''$, from Breen et al. 1994) is located 27.1 arcmin (∼1.2 h^{-1} Mpc) from the center of the cluster A3562 and 26.3 arcmin from SC 1327–312. In Fig. 7 the isodensity contours of the MECS image (in the energy range [2–10] keV) are reported, after having applied a smoothing of 6 pixels, corresponding to 0.8 arcmin. The emission from the central 8 arcmin is overplotted to the Digital Sky Survey optical image.

The isodensity contours of SC 1329–313 appear elongated with a tail pointing toward A3562. The brightest galaxy ($b_{\rm J} = 15.6$ and $v = 12\,928$ km s^{-1}) appears hosting a double nucleus. Fitting an elliptical King model, we find $r_{\rm c1} = 0.146\ h^{-1}$ Mpc, $r_{\rm c2} = 0.185\ h^{-1}$ Mpc and $\beta = 0.499$. We find also an excess of emission at ∼1.7 arcmin from the fitted center, roughly in correspondence of the brightest galaxy.

Also in this case, the Clark Clean Method deconvolution of the image leads to neglegible variations of fitted parameters. Using these values and the global temperature (see below), we estimate a mass of $M(<1\ h^{-1}$ Mpc$) \sim 5.7 \times 10^{14}\ h^{-1}\ M_\odot$, with a gas mass fraction of ∼8% $h^{-1.5}$.

The [2–10] keV luminosity is $2.36 \times 10^{43}\ h^{-2}$ erg s^{-1} and the emission in the [0.6–3] keV band is $1.17 \times 10^{43}\ h^{-2}$ erg s^{-1} within 0.5 h^{-1} Mpc from the center.

5.1. Global temperature and abundance

The global results from the region of 8 arcmin radius are $kT = 3.49^{+0.27}_{-0.24}$ keV and an abundance of $0.21^{+0.09}_{-0.11}$, with a reduced χ^2 of 0.92 with 181 degrees of freedom. We fixed the hydrogen column to 3.98×10^{20} cm^{-2} (Dickey & Lockman 1990), after having checked that it is consistent with the fitted value. Note that the addition of the LECS dataset does not significantly modify the temperature determination. The results are reported in Table 2. The derived temperature is significantly lower (at 3.3 sigma) than

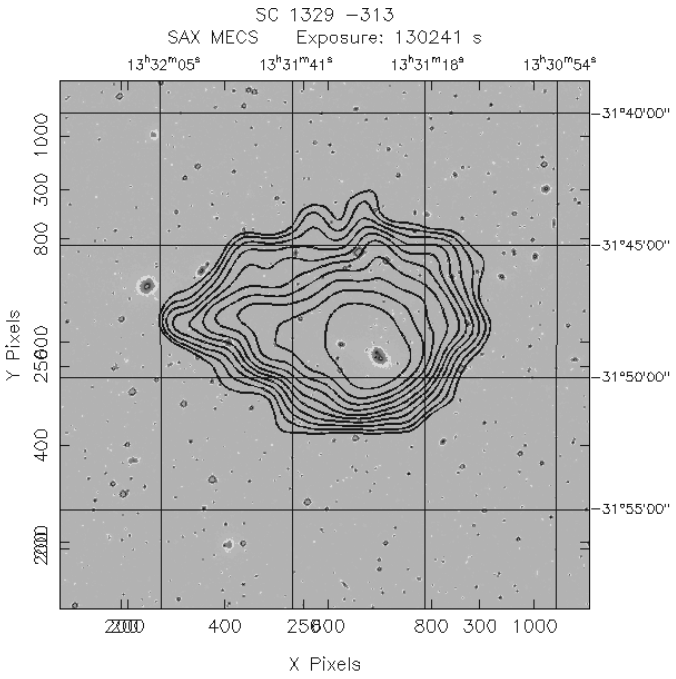

Fig. 7. MECS image of SC 1329–313 in the [2–10] keV energy range. The data have been smoothed with a Gaussian of 6 pixels, corresponding to 0.8 armin. In this figure we show the X-ray contours from the central region of 8 arcmin radius, superimposed to the Digital Sky Survey.

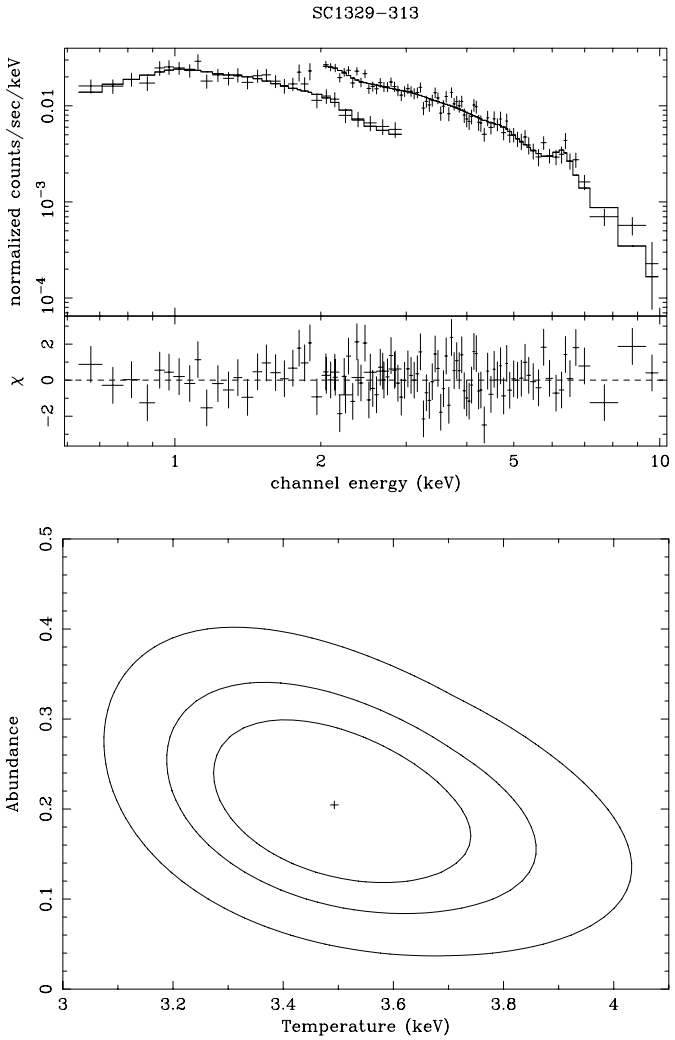

Fig. 8. Spectrum and confidence ellipse of the estimated temperature and abundance on MECS+LECS data within 8 arcmin from the center of SC 1329–313.

the ASCA determination of $kT = 4.21^{+0.15}_{-0.23}$ keV (Hanami et al. 1999): it is unclear which can be the origin of this discrepancy, given the fact that generally Beppo-SAX and ASCA results for global temperatures of clusters are in agreement (De Grandi & Molendi 2002).

In Fig. 8 we show the LECS+MECS spectrum of SC 1329–313, with overplotted the best fit, and the corresponding confidence ellipse for the temperature and abundance parameters.

The implied velocity dispersion is 702^{+33}_{-49} km s^{-1}. From the substructure analysis of Bardelli et al. (1998b) it appeared that this cluster has a bimodal velocity distribution, with the two peaks separated by ∼1500 km s^{-1} ($\langle v \rangle$ = 13 280 and 14 960 km s^{-1}) and superimposed along the line of sight. It is difficult to determine which subclump is associated with this diffuse emission. The optical substructures have centers offset by ∼9 arcmin (the farthest, T496) and ∼6 arcmin (the nearest, T520) westward. The velocity dispersions are 482^{+87}_{-49} km s^{-1} and 537^{+87}_{-32} km s^{-1}, respectively, lower than the predicted one of 2.2 and 1.6 σ. However, considering that the brightest galaxies near the X-ray emission are at ∼13 000 km s^{-1}, the group responsible for the emission is presumably T520; its position is shown in the lower panel of Fig. 1.

5.2. MECS spatially resolved spectroscopy

For this cluster we have used the same spatial binning for the concentric annuli and the same energy bands as for SC 1327–312 (see Sect. 4.2). Given the low statistics of counts, the abundance is not constrained: for this reason we choose to fix it to the global value (i.e. 0.22) for all bins. In Fig. 9, the radial temperature profile of SC 1329–313 is shown. A very marginal indication of temperature increase seems to be present.

In Fig. 10 we plot the MECS image of SC 1329–313 with overlaid thefour sectors used for the two-dimensional spectral analysis: again the contours shown in Fig. 7 correspond only to the inner part of this plot. The position angle in this case is 0 degrees, with the North-West sector pointing towards SC 1327–312 and the North-East one towards A3562. Again, in the sectors where there is a contribution from the emission of nearby objects, it is possible to extend the analysis up to 20 arcmin.

In Fig. 11 we show the temperature profiles derived for SC 1329–313 from the spectral fits for each of the 4 sectors. In all profiles we have included the temperature obtained for the central circular region with radius 2′.

We have fitted the temperature profile of sector North-West with a constant model, finding a mean temperature of 3.4 ± 0.2 keV; the temperature enhancements in the

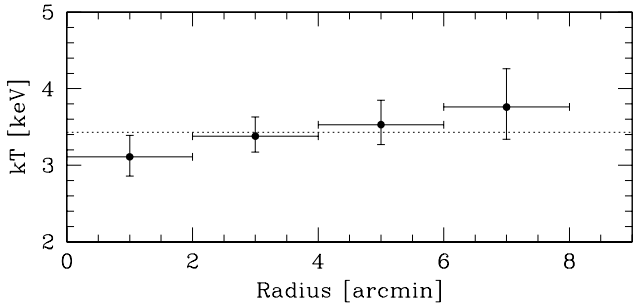

Fig. 9. Temperature radial profile of SC 1329–313. The vertical bars correspond to 68% errors, while the horizontal bars represent the bins used to extract the counts. Dotted line corresponds to the global fit.

second (2–4 arcmin) e third (4–8 arcmin) bins are statistically significant at less than 1.5σ.

In sector North-East we find X-ray emission from the cluster A3562 which is located at about 27 arcmin from the center of SC 1327–312. Ettori et al. (2000) studied the temperature map of A3562, finding a temperature of $3.9^{+1.1}_{-0.8}$ keV in the annulus 8–16 arcmin in the sector toward SC 1327–312 (sector West in Fig. 9 of Ettori et al.). This temperature is in agreement with our result in annulus 12–20 arcmin (i.e. 3.5 ± 0.3 keV), which is the region where the two cluster emissions are overlapping each others.

It appears that the increase of temperature is mainly due to the second and third bin of the NW sector (with temperatures of ∼4.5 keV). This could be an indication of the presence of heating of gas, which added to the elongation of the isophotes to the other side of SC 1329–313, are signs of interaction between this group and SC 1327–312.

Finally, given the proximity of the Beppo-SAX observations of the two poor clusters, the last three bins of the SE sector of SC 1327–312 correspond with great overlap to the last three bins of the NW sector of SC 1329–313 (see lower panel of Fig. 1). Given the fact that the two observations are statistically independent, this is an opportunity to test how robust are the temperature determinations at large radii. In Fig. 11, we plotted as squares the temperature determinations of SC 1327–312 in the corresponding bins, with a small offset on the X axis for clarity. In all bins, the two temperature estimates are very well consistent with each other.

5.3. The problem of the discrepant redshift

Hanami et al. (1999), fitting the redshift from the ASCA GIS and SIS spectrum of SC 1329–313, reported that the resulting value in not consistent with the optical value, being $z_{\rm X} < 0.031$. They found that this discrepancy is essentially due to the fact that the centroid of the iron Kα line is more consistent with H-like rather than He-like ionization. This result permitted the authors to suppose the presence also of gas at significantly higher temperature ($kT \sim 15$ keV).

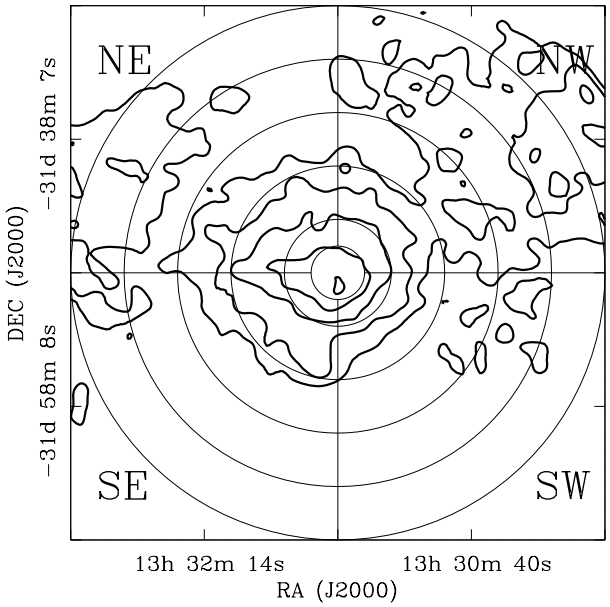

Fig. 10. Same as Fig. 5 for SC 1329–313. The position angle of the grid is zero. In this case the NW sector is pointing toward SC 1327–312 and the NE one toward A3562.

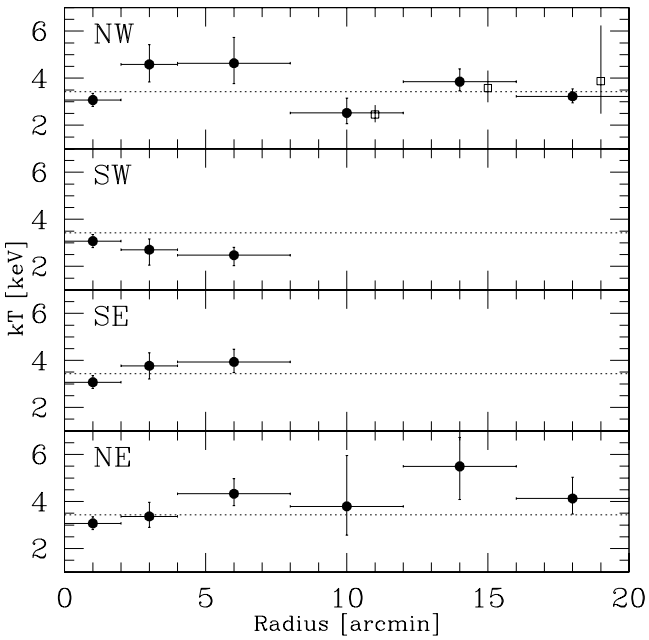

Fig. 11. Two-dimensional radial profile of the temperature of SC 1329–313. The four panels show the results of the four sectors indicated in Fig. 10. The vertical bars correspond to one sigma errors, while the horizontal bars represent the bins used to extract the counts. Dotted lines indicate the global fit values. Open squares in the last bins of the NW sector indicate the temperature estimated from the corresponding bins in the SE sector of SC 1327–312 (see text for details).

We fitted the 8 arcmin region by fixing all the parameters but the temperature, the redshift and the normalization, finding $z_{\rm fit} = 0.031$ with a 90% interval covering the range [0.019–0.049]. The result does not change by fixing the temperature. However, we have to take into account a

systematic shift of −40 eV in the channel-to-energy conversion (Fiore, private communication), resulting in a redshift shift of +0.006. Note that, within the uncertaintes and this systematic shift, the $z_{\rm fit}$ value is consistent with the mean redshift of both optical substructures (i.e. 0.044 and 0.049). The result does not change by using data in a smaller region of 5 arcmin radius.

As a further test, we fitted the spectrum with a bremsstrahlung+Gaussian model, in order to determine the centroid of the line, finding $E = 6.50$ keV with a 90% range of [6.38–6.63] keV: this result is at the border of consistency with the expected value of 6.37 keV. Considering the correction of the −40 eV on the channel-to-energy systematic offset, we found that the discrepancy is no more than 2σ of significance. As a check, we repeated this analysis also for SC 1327–312: the resulting centroid is $E = 6.37$ keV with a 90% range of [6.26–6.49] keV.

In conclusion, the evidence of presence of hotter gas in our data is weak, even if in the same direction of that found by Hanami et al. (1999), and a conclusive analysis will be possible only with the spectral capability of XMM-Newton.

6. LECS data

Recently Bonamente et al. (2001) claimed the detection in Beppo-SAX and ROSAT-PSPC data of a soft (at $E \sim 0.25$ keV) excess in the clusters A3562, A3558, A3560 and A3571. The first two clusters are part of the A3558 complex, while A3560 is $\sim 3.1\ h^{-1}$ Mpc away from SC 1329–313 and $\sim 4.1\ h^{-1}$ Mpc from SC 1327–312 and therefore could be interacting with the structure. Moreover A3571 is part of another cluster complex of the Shapley Concentration.

In principle there are no indications that this soft excess is confined in the single clusters: in fact it could be due to a diffuse, cold component (a filament) that we know to exist between A3558 and A3562 (Bardelli et al. 1996; Kull & Böhringer 1999). In order to check the possible existence of a soft excess in our LECS data, we restricted the analysis in the [0.2−0.4] keV band, considering the central region of 8 arcmin radius.

We find that the excesses in this band, with respect to the counts expected from the best fit spectrum, are 0.5 and 2.13 σ for SC 1327–312 and SC 1329–313, respectively. Considering that the values of σ are determined only by the counts statistics and not by the uncertaintes on the fit and on the calibration, we conclude that no significant excess is present in our data. Moreover, note that in Ettori et al. (2000), where a Beppo-SAX observation of A3562 was analyzed, we have not found the excess reported by Bonamente et al. (2001).

7. PDS data

There is evidence of the presence of hard X-ray excesses over a simple bremsstrahlung model in some galaxy clusters which present some degree of merging (see Fusco-Femiano 2000). These hard energy tails have been detected for the first time by the PDS instrument on board the Beppo-SAX satellite.

It is not clear what the exact mechanism is that accelerates the electrons and whether it is related to merging alone or if it requires some additional parameters (as, for instance, a preexisting radiosource or a gas temperature hotter that 6–7 keV).

For this reason it is worthwhile to investigate if an hard tail is present in our data. Following the data reduction cookbook, the main problems come from the variable background of energetic particles, which has to be subtracted. There are basically two methods to do this, i.e. the Fixed Rise Time threshold and the Variable Rise Time threshold. We checked that the counts resulting after the application of the two methods are consistent each other and give the same results. By imposing to the PDS data a *mekal* model with the same parameters fitted in the MECS alone, we find a significant excess in both SC 1327–312 and SC 1329–313 observations, in particular between 15 and 30 keV. We found $6.59 \pm 2.51 \times 10^{-2}$ cts s^{-1} against the 0.20×10^{-2} cts s^{-1} predicted by the *mekal* model for SC 1327–312 and $5.34 \pm 2.07 \times 10^{-2}$ cts s^{-1} (against 0.68×10^{-3} cts s^{-1}) for SC 1329–313. The excess flux in the two observations is consistent within the errors to be the same in the two exposures. The fit does not improve by adding a power law, which gives a formal slope ~ 3.

The spectral shape of this excess is inconsistent with the hypothesis of a cluster hard tail and indicates the presence of a contamination source. The problem in identifying the origin of this bump arises from the huge field of view of the PDS, i.e. 1.°3; our two exposures cover large part of the A3558 complex. For this reason, added to the fact that this region of the sky is poorly sampled by large X-ray surveys, it is difficult to find the possible responsible for this excess. After having checked in the literature, we found as a tentative candidate a QSO at $z = 1.335$ (Drinkwater et al. 1997; Venturi et al. 2000), located at $\alpha_{2000} = 13^{\rm h}30^{\rm m}19^{\rm s}$ and $\delta_{2000} = -31°22'59''$, i.e. North-East with respect to the position of SC 1327–312. This source was previously known as PKS1327−311 and presents a radio spectrum of steepness $\alpha_{13\rm cm}^{22\rm cm} = -1.13$ (with total flux of $S_{22\rm cm} = 421.7$ mJy, Venturi et al. 2000). This source is in the field of view of the ROSAT-PSPC observation of A3558 of Bardelli et al. 1996 with a [0.5−2.0] flux of 16.2×10^{-14} erg cm^{-2} s^{-1}.

Finally, considering the response function of the PDS instrument, the count–rate ratio between the SC 1327–312 and the SC 1329–313 observations is consistent with having been emitted by this source. In fact, the observed ratio is 1.23 ± 0.67, to be compared with the expected value of 1.32.

8. Discussion and conclusions

The aim of this work has been the study of two blobs of hot gas (SC 1327–312 and SC 1329–313) positioned between A3558 and A3562, two ACO clusters in an

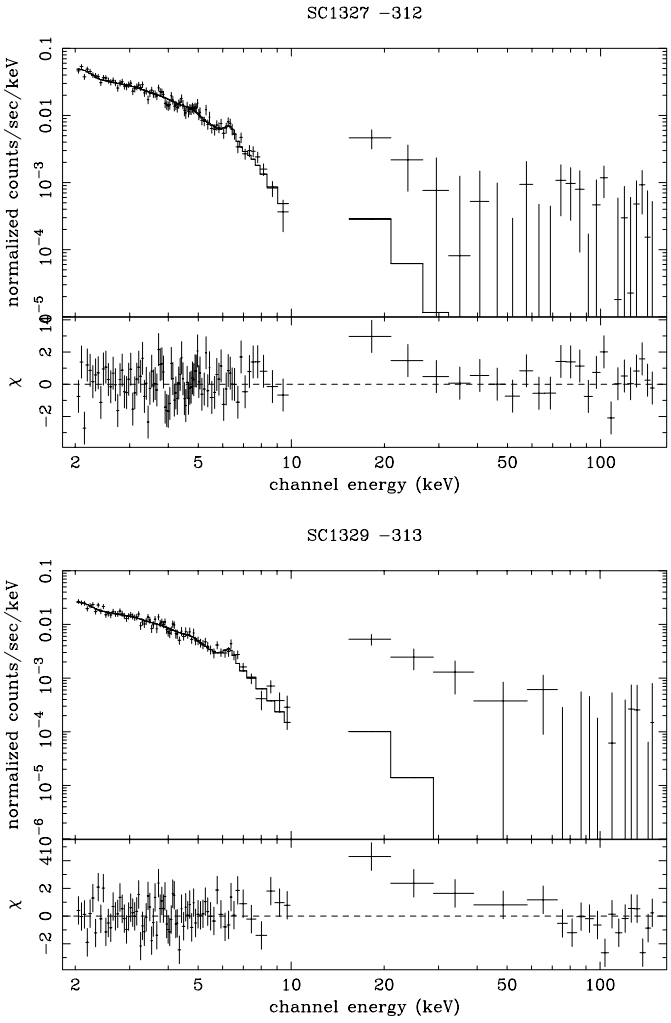

Fig. 12. PDS+MECS spectrum of SC 1327–312 (upper panel) and SC 1329–313 (lower panel).

oustanding phase of major merging. These clusters (together with A3556) form the A3558 complex, a structure with a linear dimension of $\sim 7\ h^{-1}$ Mpc at a redshift of $\sim$0.05. The relative center-to-center distance between A3562 and A3558 is $\sim 3\ h^{-1}$ Mpc.

The indication of ongoing merging comes both from the optical and from the X-ray band. From the optical band, the envelope of galaxies sorrounding the clusters cores (visible in Fig. 1; see also Fig. 2 of Bardelli et al. 1998a for the wedge diagram of the redshift sample) suggests that the galaxies from outer parts of A3562 and A3558 have been shared by the dynamical interaction. Also by studying the dynamics of the structure using redshift survey, Bardelli et al. (2000) and Reisenegger et al. (2000) concluded that the A3558 complex is at the late collapse phase. Moreover, the presence of a large number of subcondensations (Bardelli et al. 1998b) reveals that the complex is far from the relaxation.

From the X-ray, both Bardelli et al. (1996) and Kull & Böhringer (1999) detected diffuse emission extending along the whole A3558 complex, in the same way of the optical galaxies. Moreover, Markevitch & Vikhlinin (1997) found regions of hotter gas with respect to the A3558 average temperature in the direction of SC 1327–312, while Ettori et al. (2000) detected diffuse gas outside A3562, on the opposite side with respect to the A3558 direction. This picture is consistent with the results of numerical simulations of merging clusters.

In order to study the role of SC 1327–312 and SC 1329–313 in this merging picture, we analyzed two Beppo-SAX observations pointed on the centers of these two poor clusters. The MECS image of SC 1327–312 seems rather symmetric and centered on the dominant galaxy. On the contrary, the emission of SC 1329–313 has a "comet-like" shape: we detected a significant excess of X-ray emission corresponding to the position of the brightest galaxy (which appears to be double) and a tail pointing eastward. In both poor clusters, the presence of diffuse emission is visible (see Figs. 5 and 10) arising from the filament connecting the clusters of the A3558 complex. Moreover, in SC 1327–312 and SC 1329–313 images a contribution from the X-ray emission of A3558 and A3562, respectively, can be detected. These components are bright enough to allow a temperature estimate up to a distance of 20 arcmin from the frame center. Finally, possible indications of disturbance come from the displacement between the positions of the X-ray peaks and the optical substructure centroids in both objects.

We estimated the "global" (i.e. within 8 arcmin, corresponding to $\sim 0.3\ h^{-1}$ Mpc) temperatures and abundances for the two clusters using both MECS and LECS instruments. We find 4.11 keV and 0.17 for SC 1327–312 and 3.43 keV and 0.21 for SC 1329–313. These values are consistent with those expected from the velocity dispersions of the corresponding optical substructures found in Bardelli et al. (1998b).

As a further step, we performed a spatially resolved spectroscopy with the use of the MECS instrument. The temperature profiles are not very different from an isothermal distribution of the hot gas, a part from the fact that the most internal bins in the two clusters are always colder than the others. Then, we estimated the temperatures as a function of the distance from the center dividing the images in four sectors of 90°. We rotated the grids in order to have a sector of SC 1327–312 pointing toward A3558 and another toward SC 1329–313 and a sector of SC 1329–313 pointing toward A3562 and another toward SC 1327–312.

We found a good agreement between the temperatures derived in the overlapping regions of the two pointings and in the regions at the edge with A3558 and A3562, where literature estimates are available. This confirms the goodness and reproducibility of the analysis of MECS images in the most external regions, i.e. up to 20 arcmin.

We did not find evidence of the existence of a shock front inside the poor clusters, a part from a weak indication that in SC 1329–313 the temperatures in the bins between 2 and 8 arcmin in the NW sector seem to be higher than the corresponding ones in the other sectors. There appears to be a temperature increase also in most the external part of SC 1327–312 in the sector pointing

toward A3558: however, this increase is consistent with the hot region in A3558 found by Markevitch & Vikhlinin (1997).

An excess in the PDS energy range has been detected, but it turned out to be unrelated to the cluster emission and due to a contaminating source. Moreover, analysing the LECS data, we did not find a significant soft excess with respect to a single thermal bremsstrahalung.

Finally, the presence of multiphase gas in SC 1329–313, as claimed by Hanami et al. (1999) on ASCA data, has been found only at the 2σ confidence level.

In conclusion, we did not find evidence of the presence of shock-heated gas in these two poor clusters. Only SC 1329–313 presents in its distorted isophotes sign of disturbance of the hot gas: the gas profile of SC 1329–313 shows "comet-like" shaped isophotes, with the tail pointing toward A3562 and a compression toward SC 1327–312.

This is an indication that reinforces our work hypothesis: the A3558 complex is a remnant of a major merging seen after the first core-core encounter. In the numerical simulations of mergers (see for example Sarazin 2000), the shock is created between two clusters before the first collision. After the core-core encounter, the shock travels toward the external regions of the clusters, where it will be dissipated. The A3558 complex is therefore an important opportunity for studying evolved mergings and the new generation X-ray instruments (XMM-Newton and Chandra) will be helpful in order to give a complete picture of this phenomenon.

Acknowledgements. SB warmly thanks D. Dallacasa for his help with the deconvolution programs and C. Vignali and S. Pellegrini for useful discussions. We thank the referee for useful comments. This research has made use of linearized event files produced at the Beppo-SAX Science Data center. This work has been partially supported by the Italian Space Agency grants ASI-I-R-105-00 and ASI-I-R-037-01.

References

Baldi, A., Bardelli, S., & Zucca, E. 2001, MNRAS, 324, 509
Bardelli, S., Zucca, E., Vettolani, G., et al. 1994, MNRAS, 267, 665
Bardelli, S., Zucca, E., Malizia, A., et al. 1996, A&A, 305, 435
Bardelli, S., Zucca, E., Zamorani, G., Vettolani, G., & Scaramella, R. 1998a, MNRAS, 296, 599
Bardelli, S., Pisani, A., Ramella, M., Zucca, E., & Zamorani, G. 1998b, MNRAS, 300, 589
Bardelli, S., Zucca, E., Zamorani, G., Moscardini, L., & Scaramella, R. 2000, MNRAS, 312, 540
Bardelli, S., Zucca, E., & Baldi, A. 2001, MNRAS, 320, 387
Boella, G., Butler, R. C., Perola, G. C., et al. 1997a, A&AS, 122, 299
Boella, G., Chiappetti, L., Conti, G., et al. 1997b, A&AS, 122, 327
Bonamente, M., Lieu, R., Nevalainen, J., & Kaastra, J. S. 2001, ApJ, 547, L7
Breen, J., Raychaudhury, S., Forman, W., & Jones, C. 1994, ApJ, 424, 59
Colberg, J. M., White, S. D. M., Jenkins, A., & Pearce, F. R. 1999, MNRAS, 308, 593
D'Acri, F., De Grandi, S., & Molendi, S. 1998, Nucl. Phys., 69/1–3, 581
De Grandi, S., & Molendi, S. 2001, ApJ, 551, 153
De Grandi, S., & Molendi, S. 2002, ApJ, in press [astro-ph/0110469]
Dickey, J. M., & Lockman, F. J. 1990, ARA&A, 28, 215
Drinkwater, M. J., Webster, R. L., Francis, P. J., et al. 1997, MNRAS, 284, 85
Ettori, S., Fabian, A. C., & White, D. A. 1997, MNRAS, 289, 787
Ettori, S., Bardelli, S., De Grandi, S., et al. 2000, MNRAS, 318, 239
Fiore, F., Guainazzi, M., & Grandi, P. 1999, Cookbook for Beppo-SAX NFI Spectral Analysis
Fusco-Femiano, R. 2000, in Constructing the Universe with Clusters of Galaxies, ed. F. Durret, & D. Gerbal, electronic proceedings http://www.iap.fr/Conferences/Colloque/coll2000/contributions
Kaastra, J. S. 1992, An X-Ray Spectral Code for Optically Thin Plasma, Internal SRON-Leiden report, updated version 2.0
Kull, A., & Böhringer, H. 1999, A&A, 341, 23
Hanami, H., Takeshi, T., Shimasaku, K., et al. 1999, ApJ, 521, 98
Ledlow, M. J., & Owen, F. N. 1996, AJ, 112, 9
Lubin, L. M., & Bahcall, N. A. 1993, ApJ, 415, L17
Markevitch, M., & Vikhlinin, A. 1997, ApJ, 474, 84
Markevitch, M., Forman, W., Sarazin, C. L., & Vikhlinin, A. 1998, ApJ, 503, 77
Mewe, R., Kaastra, J., & Liedhal, K. 1995, Legacy, 6, 16
Parmar, A. N., Martin, D. D. E., Bavdaz, M., et al. 1997, A&AS, 122, 309
Reisenegger, A., Quintana, H., Carrasco, E. R., & Maze, J. 2000, ApJ, 120, 523
Ricker, P. M., & Sarazin, C. L. 2001, ApJ, 561, 621
Roettiger, K., Loken, C., & Burns, J. O. 1997, ApJS, 109, 307
Takizawa, M., & Mineshige, S. 1998, ApJ, 499, 82
Sarazin, C. L. 2000, in Constructing the Universe with Clusters of Galaxies, ed. F. Durret, & D. Gerbal, electronic proceedings http://www.iap.fr/Conferences/Colloque/coll2000/contributions
Venturi, T., Bardelli, S., Morganti, R., & Hunstead, R. W. 1998, MNRAS, 298, 1113
Venturi, T., Bardelli, S., Morganti, R., & Hunstead, R. W. 2000, MNRAS, 314, 594
Zucca, E., Zamorani, G., Scaramella, R., & Vettolani, G. 1993, ApJ, 407, 470